



The Polar Field Reversal Process over Five Solar Cycles Using the McIntosh Archive



The Polar Field Reversal Process over Five Solar Cycles Using the McIntosh Archive

D. F. Webb (1), B. A. Emery (2, 3), S. E. Gibson (2), I. M. Hewins (3), R. H. McFadden (3), T. A. Kuchar (1)

(1) ISR, Boston College, Chestnut Hill, MA, (2) HAO/NCAR, Boulder, CO, (3) Institute for Scientific Research (ISR), Boston College at HAO/NCAR



1. Introduction

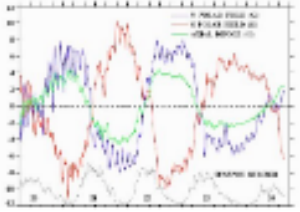
In 2004 (G20), Patrick McIntosh began creating hand-drawn magnetic maps of solar activity (Figure 1a), based on daily Ha images and magnetograms. The magnetograms were key to finding the locations of "neutral lines", or polarity-reversal lines (PRLs), that have the boundaries of opposite-polarity magnetic regions. Filaments over the Ha images, reduced the PRL locations since filaments are known to be associated with PRLs, and are more readily identified. McIntosh (2017) observed that the large-scale patterns on the surface match well the large-scale magnetic fields measured with magnetographs. His images are particularly useful for

3. A Activity Associated with Polar Magnetic Field Polarity Reversals

3.1 Evolution of the solar cycle magnetic field over 22 cycles

Clearly the period over which the reversals of the polar fields occur contains a clear seasonal information that must be explained by any successful theory. The relative timing of these reversals and the evolution of surface features associated with them over five consecutive solar cycles is the focus of this study. To provide context we show in Figure 4 the evolution of the polar field line during SCs 20, 21, 22, comparing with our study period. Also plotted is the Sun's total dipole strength. The latitude quantity is derived from a potential field source surface (PFSS) model and is representative of the evolution of the potential field component of the Sun (see e.g., Sheng & Sheng 2002; Sheng 2017). The CR averaged values from this plot are provided by Y.M. Wang and the annual values or ranges are given in Table 1, columns 4 (observed flux at each pole) and 5 (total flux for SCs 21-22).

Figure 4



4. Lag Times from Polarity Reversals and Discussion

4.1 Lag times from polarity reversals

The observations of the high-latitude events associated with each SC maximum and the polarity reversals are far separated by adding the timing of the important high-latitude events to the polarity reversals. Table 2 is derived from Table 1 and shows the lag times in CRs from the first occurrence of each polarity reversal in each hemisphere to the time of the primary PRL disappearance, the first appearance of secondary PRL in the pole, and the median persistent emergence of the pole by the next cycle CR.

2. Plotting the Median Primary and Secondary PRL Locations

Using the technique shown in Figure 1a, we construct Figure 2. This is a plot of the 2 CR averaged median values of the primary and secondary PRLs and the polar CRs from each CR map. The median primary and secondary PRL locations for each CR map are plotted as diamonds and x's for the PRL, respectively, and as squares and triangles in the SH. Red and orange values are for negative pole positions, and blue and cyan are for positive positions. The black x's are the median locations of the CR boundary lines from a CH at the pole to a 30° north-south range as average lines. The 30.00 value represents these as dashed vertical lines.

Dotted lines of the PRLs are local north-south and average for the CRs. The latitude difference between the primary and secondary PRLs are shown as blue lines by the equator for the P1 and P2, with the median difference in the more and periods as dashed lines. The dotted lines at a 30° and 22° indicate the requested limits of the primary and secondary PRLs.

Note that there were multiple PRLs in the north in SCs 20 and 21 and in the south in SC 22. These have been well documented as noted by references

5. Conclusions

The intervals in each hemisphere during which the polar fields reverse contain observational information that require explanation by any successful theory. Our study of the relative timing of these reversals and the evolution of surface features associated with them over five consecutive solar cycles provides observational context that help constrain models of the interior solar dynamo process.

The McIntosh Archive took itself to very good estimates of the evolution of the primary and secondary PRLs, and the CR locations. The "Watch the Poles" (WHP) technique enables both the primary and secondary PRLs and their not and until the secondary PRL, transitions between the primary PRL after solar maximum. For our study the disappearance of the primary PRL is key as it defines the boundary between the old cycle polar polarity and the new cycle flux between it and the secondary PRL. Thus, the disappearance of the primary PRL signals that the new cycle flux now dominates the pole. Its disappearance occurs on average about 1 year after the reversal, but

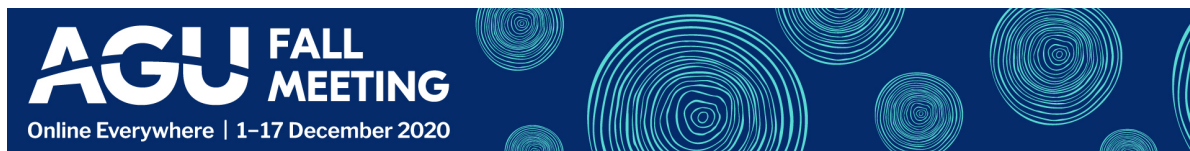
ABSTRACT REFERENCES CONTACT AUTHOR PRINT GET POSTER

D. F. Webb (1), B. A. Emery (2, 3), S. E. Gibson (2), I. M. Hewins (3), R. H. McFadden (3), T. A. Kuchar (1)

(1) ISR, Boston College, Chestnut Hill, MA, (2) HAO/NCAR, Boulder, CO, (3) Institute for Scientific Research (ISR), Boston College at HAO/NCAR



PRESENTED AT:



1. INTRODUCTION

In 1964 (SC 20), Patrick McIntosh began creating hand-drawn synoptic maps of solar activity (**Figure 1a**), based on daily H α images and magnetograms. The magnetograms were key to finding the locations of "neutral lines", or polarity inversion lines (PILs), that form the boundaries of opposite-polarity magnetic regions. Filaments on the H α images refined the PIL localization since filaments are known to be associated with PILs and are more easily distinguished. McIntosh (1979) showed that the large-scale H α patterns on the surface match well the large-scale magnetic fields measured with magnetographs. H α images are particularly useful for tracing PILs in weak field regions and near the poles of the Sun (Fox et al. 1998; McIntosh 2003). By tracing the PILs, McIntosh connected widely separated filaments to reveal the large-scale organization of the solar magnetic field. Coronal holes (CHs) were routinely added to the maps starting in 1981, primarily using ground-based He-I 10830 Å images from the National Solar Observatory at Kitt Peak. **Figure 1a** shows polar CHs during solar minimum for CR1751 in 1984. Both poles show the extension of the polar CHs to lower latitudes, creating a "gap" in the highest latitude polar crown or PIL. Webb et al. (2018) describe in detail the processing used to convert McIntosh's original hand-drawn synoptic maps to the digital maps used in this study.

We study the polar magnetic field reversal process over five solar cycles (SCs 19-23, Dec. 1954 – Aug. 2009) using the final digitized McIntosh Archive (McA) of solar synoptic maps. This data set allows the tracking of features such as filaments, PILs, CH boundaries and sunspots over many consecutive Carrington rotations. Here we follow the evolution of the polar magnetic regions of the Sun and how the Rush-to-the-Poles (RttP) and other patterns occur during the period when the polar fields reverse around each SC maximum. This process was first studied in detail for SCs 20 and 21 by Webb et al. (1984). The goal then as now is to use the RttP and CH boundary mapping to better constrain solar interior and dynamo models. We use the McA data set to determine the timing and lags for these events around each SC maximum at each pole: the sunspot number peak, the magnetic polarity reversal, the disappearance of the primary PIL, the first appearance at the pole of the CH of new-cycle polarity, and the earliest persistent full coverage of each pole by a coronal hole. With the newly processed McA, we can now extend this type of study over five consecutive SCs, 19-23.

Figure 1a

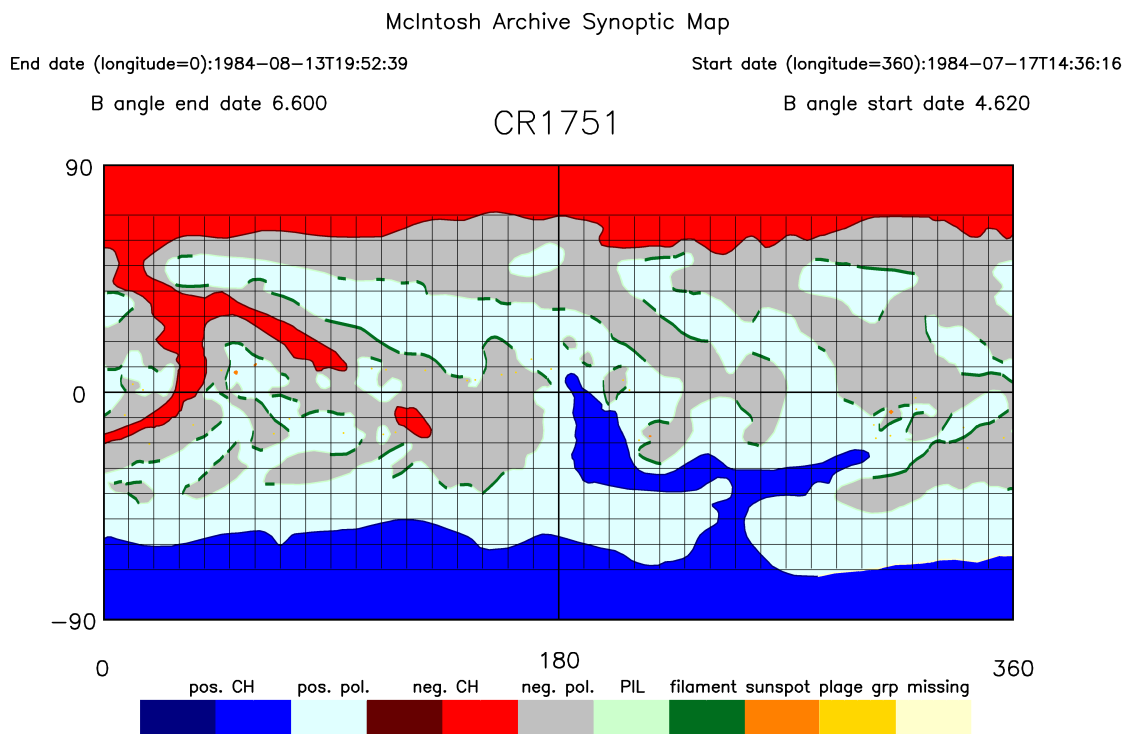
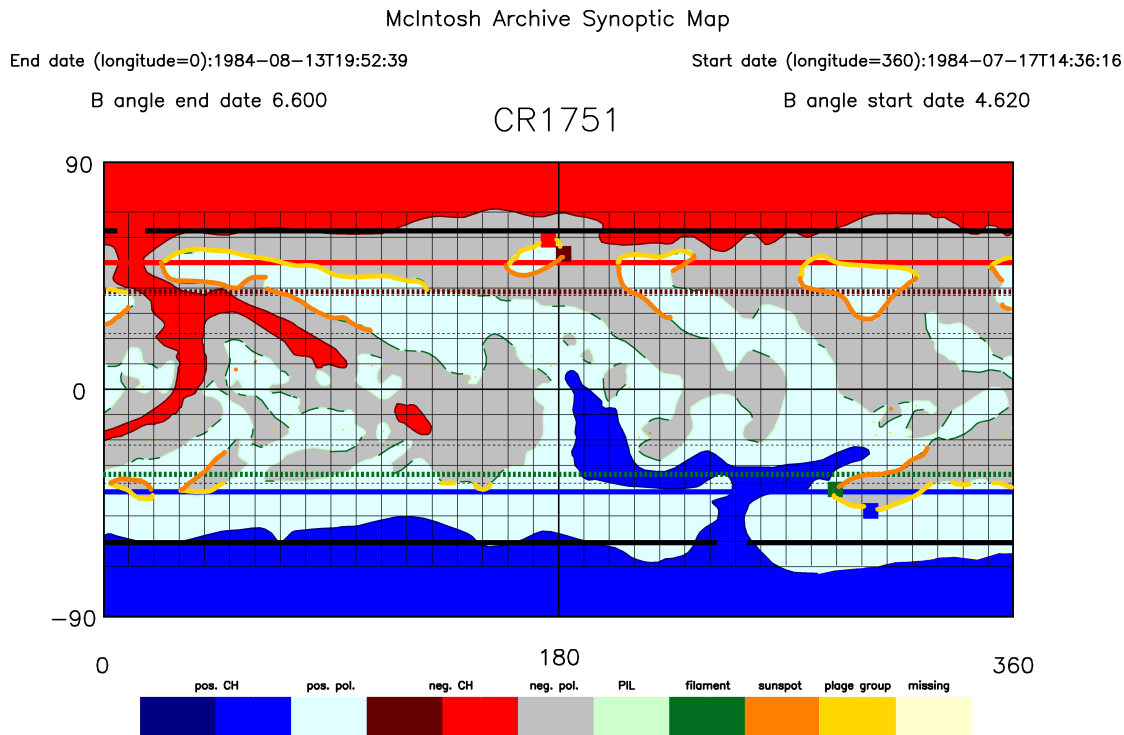


Figure 1a shows a McA map of CR1751 in SC 21 during solar minimum. The PILs are shown in pale green with filaments in thick, dark green segments of the PILs. CHs from He-I 10830 Å images are in red for the negative north hemisphere (NH) pole and blue for the positive south hemisphere (SH) pole. Active plage regions in orange and gold spots near the equator denote

plage regions and large sunspots, respectively.

Figure 1b



To illustrate our technique, we show in **Figure 1b** the same map with primary PILs overdrawn in gold and secondary PILs in orange where primaries can only go to $\pm 37^\circ$ and secondaries to $\pm 22^\circ$ (light dashed lines). The median values of the primary PILs are a thick horizontal solid blue (positive pole) line in the SH and red (negative pole) in the NH. Thick horizontal dotted lines show the median locations of the secondary PILs in dark red and green. The polemost latitude PIL locations for this CR are squares in the same colors. The thick, solid horizontal black lines at 62.5°N and 60.5°S are the medians of the NH and SH polar CH boundaries found equatorward from a polar CH to $\pm 50^\circ$.

2. PLOTTING THE MEDIAN PRIMARY AND SECONDARY PIL LOCATIONS

Using the technique shown in **Figure 1b**, we construct **Figure 2**. This is a plot of the 3-CR smoothed median values of the primary and secondary PILs and the polar CHs from each CR map. The median primary and secondary PIL locations for each CR map are plotted as diamonds and x's for the NH, respectively, and as asterisks and triangles in the SH. Red and orange colors are for negative pole polarities, and blue and cyan are for positive polarities. The black +'s are the median locations of the CH boundary found from a CH at the pole to $\pm 50^\circ$ with fitted slopes as orange lines. The SILSO solar minimum times are dashed vertical lines.

Fitted slopes of the PILs are black solid lines and orange for the CHs. The latitude difference between the primary and secondary PILs are shown as blue lines by the equator for the NH and SH, with the median differences in the non-rush periods as dashed lines. The dotted lines at $\pm 37^\circ$ and $\pm 22^\circ$ indicate the equatorward limits of the primary and secondary PILs.

Note that there were multiple RttPs in the north in SCs 19 and 20 and in the south in SC 22. These have been well documented as caused by poleward surges in the meridional flow of trailing opposite polarity flux from earlier emerging regions (e.g., Petrie 2015).

Figure 2

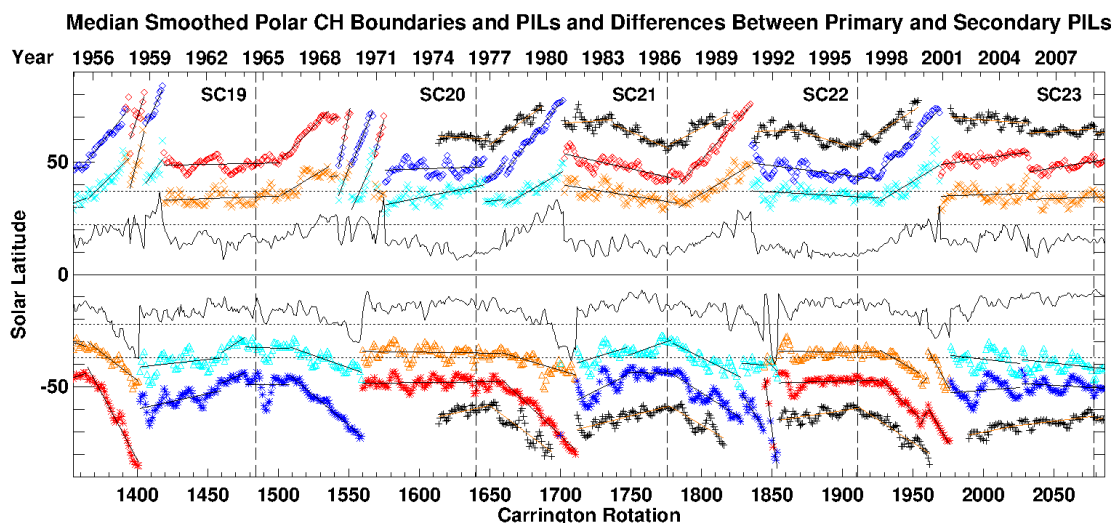
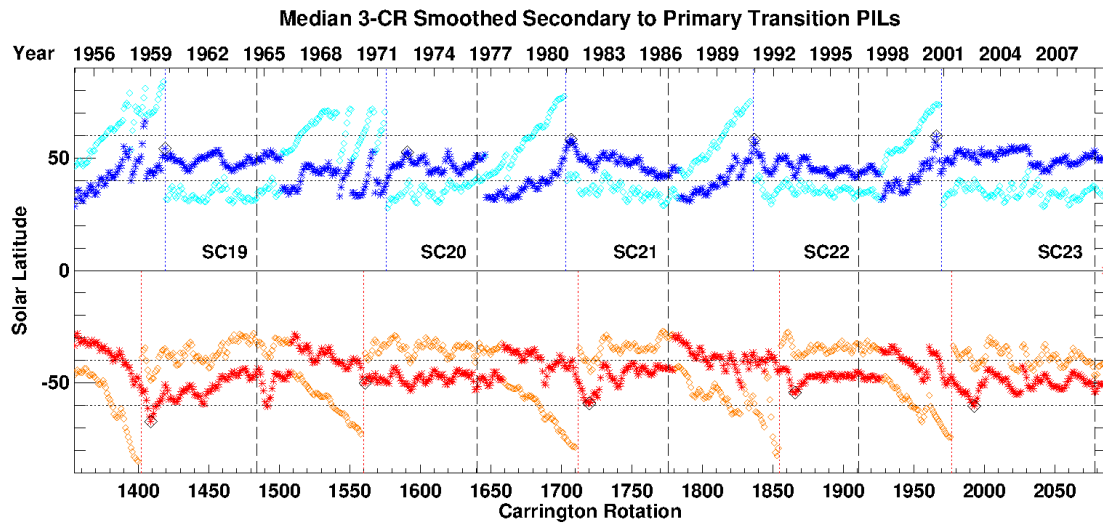


Figure 3 is a simpler version of **Figure 2** without the CH boundary and difference data. This shows how the transition from secondary to primary PIL locations occurs over two consecutive SCs, or 22 years. The sunspot solar minima are vertical black dashed lines, while the median polarity changes at the poles are blue and red dotted lines in the NH and SH, respectively. The transition peaks are marked with vertical yellow lines, which can be masked by the polarity change lines.

The merging of the secondary RttP to become the primary non-rush period are asterisks in blue (NH) and red (SH). The cyan (NH) and orange (SH) diamonds are the initial secondary non-rush period and the final primary RttP with multiple RttPs also shown with secondary PIL asterisks and primary PIL diamonds.

Figure 3



3. ACTIVITY ASSOCIATED WITH POLAR MAGNETIC FIELD POLARITY REVERSALS

3.1 Evolution of the solar polar magnetic fields over SCs 19-23

Clearly the period over which the reversals of the polar fields occur contains observational information that must be explained by any successful theory. The relative timing of these reversals and the evolution of surface features associated with them over five consecutive solar cycles is the focus of this study. To provide context we show in **Figure 4** the evolution of the polar field flux during SCs 20-24, overlapping with our study period. Also plotted is the Sun's axial dipole strength. This latter quantity is derived from a potential-field-source-surface (PFSS) model and is representative of the evolution of the poloidal field component of the Sun (see, e.g., Wang & Sheeley 2002; Wang 2017). The CR-averaged values from this plot were provided by Y-M Wang and the reversal times or ranges are given in **Table 1**, columns 4 (observed flux at each pole) and 5 (axial flux for SCs 21-23).

Figure 4

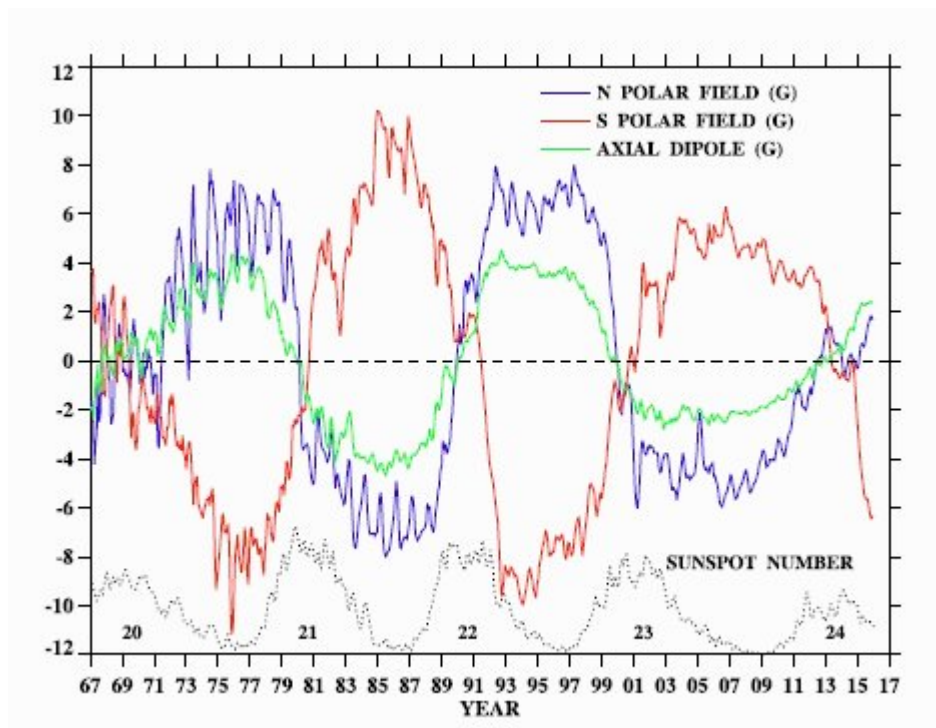


Figure 4 shows the evolution of the Sun's polar fields from 1967–2015, derived from Mt. Wilson Observatory and Wilcox Solar Observatory observations and averaged together during their period of overlap (1976–2012). The curves show the mean flux density in Gauss poleward of latitude $|L|=60^\circ$ in each hemisphere (blue: north pole; red: south pole). Also plotted is the Sun's axial dipole strength (green). The sunspot number is shown by the black dotted line. All curves represent 3-CR running means. From Wang (2017).

3.2 Polar events at activity maximum associated with polarity reversals

In **Table 1** we list for each SC and hemisphere the high-latitude events around each activity maximum that were associated with each polarity reversal. In columns 2, 3, and 4 we list which hemisphere, the CR of the sunspot peak, and the CR(s) of the polarity reversal $> 70^\circ$, respectively. The hemisphere that switched first in each cycle is listed first. The reversal sequence began first in the SH for SCs 19-20, and the NH precedes the SH for SCs 21-23. The sunspot numbers are the SILSO 13-month moving averages of the monthly numbers for each hemisphere from the Royal Observatory of Belgium's Uccle station before 1992, and from a world-wide network afterwards (<http://www.sidc.be/silso/datafiles> (<http://www.sidc.be/silso/datafiles>)).

The last 3 columns provide the CR(s) of the disappearance of the primary PIL, the first appearance of a new-cycle polarity CH at the pole, and the earliest persistent complete coverage of the pole by the new-cycle CH, respectively. Note that CHs were not observed before SC 20.

Table 1

Cycle No.	Pole ¹	CR-SSN Peak ²	CR-Polarity Reversal > 70° lat. ³	CR-Pol. Rev. of Axial Dipole ⁴	CR-Disappearance of Primary PIL ⁵	CR-First Polar CH Appear. ⁶	CR-Pole First Covered by New-cycle CH ⁷
19	SH	1391	1385-1389	---	1405	---	---
19	NH	1411	1407	---	1420	---	---
20	SH	1553	1552	---	1561	<1601 (~1560)	<1601 (1563-1567)
20	NH	1544	1563 (1577)	---	1576	<1601 (≤1567)	<1601 (1572-1573)
21	NH	1688	1691	1687	1703	1702	1712 (1711-1712)
21	SH	1691	1698		1712	1712	1717
22	NH	1815	1821-1828	1823	1836	1836	1843
22	SH	1835	1821-1844		1855	1848-1854	1857
23	NH	1970	1957	1951-1958	1970	1970	1978
23	SH	1986	1952-1976		1977	1989	1990

Key:

¹ = The first pole listed in each cycle switched polarity first.

² = From SILSO 13-month running mean sunspot numbers (Emery et al. [2020] Table 1b, col. 2).

³ = SC 19 and 20 from Webb et al. (1984), Table 1; SC 21-23 from Y. Wang (WSO data - priv. comm., 2020)

⁴ = SC 21-23 from Y. Wang (WSO data - priv. comm., 2020); Axial dipole data based on PFSS model (Wang & Sheeley, 2002).

⁵ = From Emery et al. (2020, in prep.) Table 2, col. 2.

⁶ = From McA CR Level 3 gif images; () from HAO Mk2 Synoptic Maps (A. Lecinski, priv. comm., 2019).

⁷ = From Emery et al. (2020, in prep.); () from Webb et al. (1984), Table 1.

4. LAG TIMES FROM POLARITY REVERSALS AND DISCUSSION

4.1 Lag times from polarity reversals

The observations of the high-latitude events associated with each SC maximum and the polarity reversals can be organized by relating the timing of the important high-latitude events to the polarity reversals. **Table 2** is derived from **Table 1** and shows the lag times in CRs from the time or range of each polarity reversal in each hemisphere to the time of the primary PIL disappearance, the first appearance of a new-cycle polarity CH at the pole, and the earliest persistent complete coverage of the pole by the new-cycle CH.

Table 2

Cycle No.	Pole	Lag to PIL Disappearance (CRs)	Lag to First Polar CH Appearance (CRs)	Lag to First Full Coverage of Pole (CRs)
19	S	+16-20	---	---
19	N	+13	---	---
20	S	+9	>+9 (~+8)	>+9 (+11-15)
20	N	+13 (-1)	>+9 (≥+4)	>+9 (+9-10)
21	N	+12	+11	+21
21	S	+14	+14	+19
22	N	+8-15	+8-15	+15-22
22	S	+11-34	+4-33	+13-36
23	N	+13	+13	+21
23	S	+1-25	+13-37	+14-38

4.2 Discussion

We summarize these results for the 5 SCs as follows:

From **Table 1** we see that in general the peak time of flux emergence, as signified by the sunspot number peak, is not consistently ahead of or behind the polar reversal time. Generally, the flux peak occurs before or around the same time as the reversal, but in SC 23 it was a year or so later. (However, SC 23 was an anomalously long cycle.)

From **Table 2** we note that the final disappearance of the polemost, or “primary” PIL, typically lags the polarity reversal by 8 months to 2 years. The disappearance of the PILs is clearly related to that of polar crown filaments, which Webb et al (1984) found to lag the polarity reversal from 8 mo. to 1.5 years in SCs 19-21. This timing is also similar to the appearance at the pole of the first CH of new-cycle polarity. Finally, complete CH coverage of the pole occurred about 1-2 years after the reversal.

5. CONCLUSIONS

The intervals in each hemisphere during which the polar fields reverse contain observational information that must be explained by any successful theory. Our study of the relative timing of these reversals and the evolution of surface features associated with them over five consecutive solar cycles provides observational context that help constrain models of the interior solar dynamo process.

The McIntosh Archive lends itself to very good estimates of the evolution of the primary and secondary PILs, and the CH boundaries. The “Rush-to-the-Poles” (RtTP) behavior involves both the primary and secondary PILs and does not end until the secondary PIL transitions to become the primary PIL after solar maximum. For our study the disappearance of the primary PIL is key as it forms the boundary between the old-cycle polar polarity and the new-cycle flux between it and the secondary PIL. Thus, the disappearance of the primary PIL signals that the new-cycle flux now dominates the pole. Its disappearance occurs on average about 1 year after the reversal, but ranges from 8 mo. up to 2 years later.

During the RtTPs, the primary and secondary PILs average $\sim 14^\circ$ apart in latitude, and share common features in each hemisphere. The CH boundaries lie $\sim 16^\circ$ poleward of the primary PIL. Our results compare favorably with the previous work with an earlier version of the archive (e.g., McIntosh, 2003), except we see an increase in the primary to secondary latitude differences from beginning to end of the RtTP. Our new results using median locations show a polemost limit to the primary PIL at $\sim 75^\circ$ latitude in the NH and $\sim 78^\circ$ in the SH.

The polar CHs retreat, or decrease in area, during each RtTP, starting within 1-2 CRs “simultaneously” in both hemispheres (**Figure 2**). The PIL RtTP usually starts 5-15 CRs later than that of the polar holes. The polar CHs then disappear during the polarity reversal but before the primary PIL disappears. The CHs begin to reappear with new-cycle polarity from 8 mo. to 1.5 years after the magnetic reversal, and completely cover the poles about 1-2 years after the reversal.

Information about the McIntosh Archive and access to the data set is available at:

<https://www2.hao.ucar.edu/mcintosh-archive/four-cycles-solar-synoptic-maps> (<https://www2.hao.ucar.edu/mcintosh-archive/four-cycles-solar-synoptic-maps>)

ABSTRACT

We study the polar magnetic field reversal process over five solar cycles (SCs 19-23, Dec. 1954 – Aug. 2009) using the recently digitized McIntosh Archive (McA) of solar synoptic maps. This data set allows the tracking of features such as filaments, polarity inversion lines (PILs), coronal hole boundaries and sunspots over many consecutive Carrington rotations. Here we follow the evolution of the polar magnetic regions of the Sun and how the rush-to-the-poles and other patterns occur during the period when the polar fields reverse around each SC maximum. This process was first studied in detail for SCs 20 and 21 by Webb et al. (1984). The goal then as now is to use the rush-to-the-poles and CH boundary mapping to better constrain solar interior and dynamo models. We use the McA data sets to determine the timing and lags among these events around the maximum of each SC in each hemisphere: the sunspot number peak, the polarity reversal, the disappearance of the polar crown filaments and PIL, the first appearance of mid-latitude CHs of new-cycle polarity, and the earliest complete coverage of each pole by a coronal hole. With the newly processed McA, we can now extend this type of study over five consecutive SCs through SC 23.

REFERENCES

Emery, B.A. et al., Latitude Variations in Primary and Secondary Polar Crown Polarity Inversion

Lines and Polar Coronal Hole Boundaries over Five Solar Cycles, in prep., 2020

Fox, P., P. McIntosh, and P.R. Wilson, Sol. Phys., 177, 375-393, 1998

McIntosh, P.S., UAG-70, World Data Center A for Solar-Terrestrial Physics, NOAA Space

Environment Laboratory, Boulder, CO, 1979.

McIntosh, P.S., in Solar Variability as an Input to the Earth's Environment, A. Wilson (ed.),

ESA SP-535, ESTEC, Noordwijk, Netherlands, 807, 2003.

Petrie, G. J. D., LRSP, 12, 5, 2015.

Wang, Y.-M. & N.R. Sheeley, Jr., JGR, 107, A10 1302, 2002

Wang, Y.-M., Space Sci. Rev., 210, 351, 2017

Webb, D.F., J.M. Davis & P.S. McIntosh, Sol. Phys., 92, 109, 1984.

Webb, D.F., S.E. Gibson, I.M. Hewins, R.H. McFadden, B. A. Emery, A. Malanushenko & T.A.

Kuchar, Front. Astron. Space Sci., 5, 23, 2018.